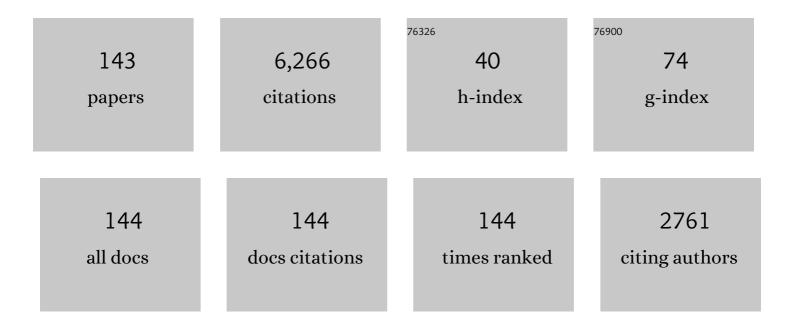
Jerry Goldstein

List of Publications by Year in descending order

Source: https://exaly.com/author-pdf/5609517/publications.pdf Version: 2024-02-01



#	Article	IF	CITATIONS
1	Electron-scale measurements of magnetic reconnection in space. Science, 2016, 352, aaf2939.	12.6	545
2	Science Goals and Overview of the Radiation Belt Storm Probes (RBSP) Energetic Particle, Composition, and Thermal Plasma (ECT) Suite on NASA's Van Allen Probes Mission. Space Science Reviews, 2013, 179, 311-336.	8.1	463
3	An extreme distortion of the Van Allen belt arising from the â€~Hallowe'en' solar storm in 2003. Nature, 2004, 432, 878-881.	27.8	299
4	Ionospheric signatures of plasmaspheric tails. Geophysical Research Letters, 2002, 29, 1-1.	4.0	270
5	A Long-Lived Relativistic Electron Storage Ring Embedded in Earth's Outer Van Allen Belt. Science, 2013, 340, 186-190.	12.6	216
6	The Two Wide-angle Imaging Neutral-atom Spectrometers (TWINS) NASA Mission-of-Opportunity. Space Science Reviews, 2009, 142, 157-231.	8.1	170
7	Extreme Ultraviolet Imager Observations of the Structure and Dynamics of the Plasmasphere. Space Science Reviews, 2003, 109, 25-46.	8.1	159
8	Global response of the plasmasphere to a geomagnetic disturbance. Journal of Geophysical Research, 2003, 108, .	3.3	144
9	Identifying the plasmapause in IMAGE EUV data using IMAGE RPI in situ steep density gradients. Journal of Geophysical Research, 2003, 108, .	3.3	130
10	Simultaneous remote sensing and in situ observations of plasmaspheric drainage plumes. Journal of Geophysical Research, 2004, 109, .	3.3	127
11	Control of plasmaspheric dynamics by both convection and sub-auroral polarization stream. Geophysical Research Letters, 2003, 30, .	4.0	117
12	Plasmaspheric Density Structures and Dynamics: Properties Observed by the CLUSTER and IMAGE Missions. Space Science Reviews, 2009, 145, 55-106.	8.1	109
13	Simulated magnetopause losses and Van Allen Probe flux dropouts. Geophysical Research Letters, 2014, 41, 1113-1118.	4.0	105
14	Observations of coincident EMIC wave activity and duskside energetic electron precipitation on 18–19 January 2013. Geophysical Research Letters, 2015, 42, 5727-5735.	4.0	102
15	IMF-driven plasmasphere erosion of 10 July 2000. Geophysical Research Letters, 2003, 30, .	4.0	95
16	Simulation of Van Allen Probes plasmapause encounters. Journal of Geophysical Research: Space Physics, 2014, 119, 7464-7484.	2.4	95
17	IMF-driven overshielding electric field and the origin of the plasmaspheric shoulder of May 24, 2000. Geophysical Research Letters, 2002, 29, 66-1-66-4.	4.0	91
18	Global plasmasphere evolution 22â \in "23 April 2001. Journal of Geophysical Research, 2005, 110, .	3.3	91

#	Article	IF	CITATIONS
19	Coupled response of the inner magnetosphere and ionosphere on 17 April 2002. Journal of Geophysical Research, 2005, 110, .	3.3	85
20	Magnetospheric model of subauroral polarization stream. Journal of Geophysical Research, 2005, 110, .	3.3	85
21	Global-scale coherence modulation of radiation-belt electron loss from plasmaspheric hiss. Nature, 2015, 523, 193-195.	27.8	83
22	Investigation of EMIC wave scattering as the cause for the BARREL 17 January 2013 relativistic electron precipitation event: A quantitative comparison of simulation with observations. Geophysical Research Letters, 2014, 41, 8722-8729.	4.0	78
23	Radiation belt electron acceleration during the 17 March 2015 geomagnetic storm: Observations and simulations. Journal of Geophysical Research: Space Physics, 2016, 121, 5520-5536.	2.4	77
24	Electron density in the magnetosphere. Journal of Geophysical Research, 2004, 109, .	3.3	76
25	Field line dependence of magnetospheric electron density. Geophysical Research Letters, 2002, 29, 58-1-58-4.	4.0	72
26	The global pattern of evolution of plasmaspheric drainage plumes. Geophysical Monograph Series, 2005, , 1-22.	0.1	69
27	Latitudinal density dependence of magnetic field lines inferred from Polar plasma wave data. Journal of Geophysical Research, 2001, 106, 6195-6201.	3.3	64
28	Cause of plasmasphere corotation lag. Geophysical Research Letters, 2004, 31, n/a-n/a.	4.0	62
29	Characterizing cometary electrons with kappa distributions. Journal of Geophysical Research: Space Physics, 2016, 121, 7407-7422.	2.4	62
30	Plasmasphere Response: Tutorial and Review of Recent Imaging Results. Space Science Reviews, 2007, 124, 203-216.	8.1	56
31	Periodicity in Saturn's magnetosphere: Plasma cam. Geophysical Research Letters, 2009, 36, .	4.0	56
32	Magnetospheric electron density model inferred from Polar plasma wave data. Journal of Geophysical Research, 2002, 107, SMP 25-1.	3.3	54
33	Dynamic relationship between the outer radiation belt and the plasmapause during March–May 2001. Geophysical Research Letters, 2005, 32, .	4.0	53
34	Two Wideâ€Angle Imaging Neutralâ€Atom Spectrometers and Interstellar Boundary Explorer energetic neutral atom imaging of the 5 April 2010 substorm. Journal of Geophysical Research, 2012, 117, .	3.3	51
35	Plasmaspheric depletion, refilling, and plasmapause dynamics: A coordinated ground-based and IMAGE satellite study. Journal of Geophysical Research, 2006, 111, .	3.3	50
36	Recent Progress in Physics-Based Models ofÂtheÂPlasmasphere. Space Science Reviews, 2009, 145, 193-229.	8.1	50

#	Article	IF	CITATIONS
37	Sounding of the plasmasphere by Mid ontinent MAgnetoseismic Chain (McMAC) magnetometers. Journal of Geophysical Research: Space Physics, 2013, 118, 3077-3086.	2.4	44
38	Comparison of TWINS images of lowâ€altitude emission of energetic neutral atoms with DMSP precipitating ion fluxes. Journal of Geophysical Research, 2010, 115, .	3.3	43
39	Magnetospheric ion influence on magnetic reconnection at the duskside magnetopause. Geophysical Research Letters, 2016, 43, 1435-1442.	4.0	42
40	A coordinated ground-based and IMAGE satellite study of quiet-time plasmaspheric density profiles. Geophysical Research Letters, 2003, 30, .	4.0	41
41	Ring current dynamics in moderate and strong storms: Comparative analysis of TWINS and IMAGE/HENA data with the Comprehensive Ring Current Model. Journal of Geophysical Research, 2010, 115, .	3.3	39
42	Evolution of lowâ€altitude and ring current ENA emissions from a moderate magnetospheric storm: Continuous and simultaneous TWINS observations. Journal of Geophysical Research, 2010, 115, .	3.3	39
43	Storm-time penetration electric fields and their effects. Eos, 2006, 87, 131.	0.1	38
44	First IBEX observations of the terrestrial plasma sheet and a possible disconnection event. Journal of Geophysical Research, 2011, 116, n/a-n/a.	3.3	38
45	Analyzing electric field morphology through data-model comparisons of the Geospace Environment Modeling Inner Magnetosphere/Storm Assessment Challenge events. Journal of Geophysical Research, 2006, 111, .	3.3	37
46	Magnetospheric electron density longâ€ŧerm (>1 day) refilling rates inferred from passive radio emissions measured by IMAGE RPI during geomagnetically quiet times. Journal of Geophysical Research, 2012, 117, .	3.3	35
47	The plasma environment inside geostationary orbit: A Van Allen Probes HOPE survey. Journal of Geophysical Research: Space Physics, 2017, 122, 9207-9227.	2.4	34
48	Plasmapause undulation of 17 April 2002. Geophysical Research Letters, 2004, 31, .	4.0	33
49	Five Years of Stereo Magnetospheric Imaging by TWINS. Space Science Reviews, 2013, 180, 39-70.	8.1	33
50	The TWINS exospheric neutral H-density distribution under solar minimum conditions. Annales Geophysicae, 2011, 29, 2211-2217.	1.6	32
51	In situ signatures of residual plasmaspheric plumes: Observations and simulation. Journal of Geophysical Research: Space Physics, 2014, 119, 4706-4722.	2.4	32
52	Multiâ€instrument analysis of plasma parameters in Saturn's equatorial, inner magnetosphere using corrections for spacecraft potential and penetrating background radiation. Journal of Geophysical Research: Space Physics, 2014, 119, 3683-3707.	2.4	32
53	Magnetospheric ion influence at the dayside magnetopause. Journal of Geophysical Research: Space Physics, 2017, 122, 8617-8631.	2.4	32
54	On the cause of Saturn's plasma periodicity. Geophysical Research Letters, 2008, 35, .	4.0	31

#	Article	IF	CITATIONS
55	Evolution of CIR storm on 22 July 2009. Journal of Geophysical Research, 2012, 117, .	3.3	30
56	Effects of modeled ionospheric conductance and electron loss on selfâ€consistent ring current simulations during the 5–7 April 2010 storm. Journal of Geophysical Research: Space Physics, 2015, 120, 5355-5376.	2.4	29
57	The response of the HÂgeocorona between 3 and 8â€ <i>R</i> _e to geomagnetic disturbances studied using TWINS stereo Lyman- <i>α</i> data. Annales Geophysicae. 2017. 35. 171-179.	1.6	29
58	Multipoint observations of ionic structures in the plasmasphere by CLUSTER—CIS and comparisons with IMAGE-EUV observations and with model simulations. Geophysical Monograph Series, 2005, , 23-53.	0.1	27
59	Simulation and TWINS observations of the 22 July 2009 storm. Journal of Geophysical Research, 2010, 115, .	3.3	26
60	Remote observations of ion temperatures in the quiet time magnetosphere. Geophysical Research Letters, 2011, 38, n/a-n/a.	4.0	26
61	Crossâ€scale observations of the 2015 St. Patrick's day storm: THEMIS, Van Allen Probes, and TWINS. Journal of Geophysical Research: Space Physics, 2017, 122, 368-392.	2.4	25
62	In situ and ground-based intercalibration measurements of plasma density atL= 2.5. Journal of Geophysical Research, 2003, 108, .	3.3	24
63	Electric fields deduced from plasmapause motion in IMAGE EUV images. Geophysical Research Letters, 2004, 31, .	4.0	24
64	Ground magnetometer observation of a crossâ€phase reversal at a steep plasmapause. Journal of Geophysical Research, 2007, 112, .	3.3	23
65	Field line distribution of density at <l>L</l> =4.8 inferred from observations by CLUSTER. Annales Geophysicae, 2009, 27, 705-724.	1.6	22
66	TWINS stereoscopic imaging of multiple peaks in the ring current. Journal of Geophysical Research: Space Physics, 2015, 120, 368-383.	2.4	22
67	Variations of oxygen charge state abundances in the global magnetosphere, as observed by Polar. Journal of Geophysical Research: Space Physics, 2016, 121, 1091-1113.	2.4	22
68	The Warm Plasma Composition in the Inner Magnetosphere During 2012–2015. Journal of Geophysical Research: Space Physics, 2017, 122, 11,018.	2.4	22
69	Observations of the ionospheric projection of the plasmapause. Geophysical Research Letters, 2008, 35, .	4.0	21
70	Oxygenâ€hydrogen differentiated observations from TWINS: The 22 July 2009 storm. Journal of Geophysical Research: Space Physics, 2013, 118, 3377-3393.	2.4	21
71	Evolution of mass density and O+ concentration at geostationary orbit during storm and quiet events. Journal of Geophysical Research: Space Physics, 2014, 119, 6417-6431.	2.4	21
72	Overshielding event of 28-29 July 2000. Geophysical Research Letters, 2003, 30, .	4.0	20

#	Article	IF	CITATIONS
73	Plasmaspheric Density Structures and Dynamics: Properties Observed by the CLUSTER and IMAGE Missions. , 2009, , 55-106.		20
74	Comparative analysis of low-altitude ENA emissions in two substorms. Journal of Geophysical Research: Space Physics, 2013, 118, 724-731.	2.4	20
75	TWINS energetic neutral atom observations of localâ€timeâ€dependent ring current anisotropy. Journal of Geophysical Research, 2012, 117, .	3.3	19
76	Large magnetic storms as viewed by TWINS: A study of the differences in the medium energy ENA composition. Journal of Geophysical Research: Space Physics, 2014, 119, 2819-2835.	2.4	19
77	Wave Phenomena and Beamâ€Plasma Interactions at the Magnetopause Reconnection Region. Journal of Geophysical Research: Space Physics, 2018, 123, 1118-1133.	2.4	19
78	Quantitative test of the cavity resonance explanation of plasmaspheric Pi2 frequencies. Journal of Geophysical Research, 2002, 107, SMP 4-1.	3.3	18
79	Global images of trapped ring current ions during main phase of 17 March 2015 geomagnetic storm as observed by TWINS. Journal of Geophysical Research: Space Physics, 2016, 121, 6509-6525.	2.4	18
80	The relationship between the plasmapause and outer belt electrons. Journal of Geophysical Research: Space Physics, 2016, 121, 8392-8416.	2.4	18
81	Storm time empirical model of O ⁺ and O ⁶⁺ distributions in the magnetosphere. Journal of Geophysical Research: Space Physics, 2017, 122, 8353-8374.	2.4	18
82	Longitudinal Structure of Oxygen Torus in the Inner Magnetosphere: Simultaneous Observations by Arase and Van Allen Probe A. Geophysical Research Letters, 2018, 45, 10,177.	4.0	18
83	Simultaneous identification of a plasmaspheric plume by a ground magnetometer pair and IMAGE Extreme Ultraviolet Imager. Journal of Geophysical Research, 2006, 111, .	3.3	17
84	Ground and satellite observations of low″atitude red auroras at the initial phase of magnetic storms. Journal of Geophysical Research: Space Physics, 2013, 118, 256-270.	2.4	17
85	Oxygen torus and its coincidence with EMIC wave in the deep inner magnetosphere: Van Allen Probe B and Arase observations. Earth, Planets and Space, 2020, 72, 111.	2.5	17
86	Magnetic latitude dependence of oxygen charge states in the global magnetosphere: Insights into solar wind-originating ion injection. Journal of Geophysical Research: Space Physics, 2016, 121, 9888-9912.	2.4	16
87	Temperature Dependence of Plasmaspheric Ion Composition. Journal of Geophysical Research: Space Physics, 2019, 124, 6585-6595.	2.4	16
88	Epochâ€Based Model for Stormtime Plasmapause Location. Journal of Geophysical Research: Space Physics, 2019, 124, 4462-4491.	2.4	16
89	Comparison of TWINS and THEMIS observations of proton pitch angle distributions in the ring current during the 29 May 2010 geomagnetic storm. Journal of Geophysical Research: Space Physics, 2013, 118, 4895-4905.	2.4	15
90	Modeling Inner Magnetospheric Electric Fields: Latest Self-Consistent Results. Geophysical Monograph Series, 0, , 263-269.	0.1	14

#	Article	IF	CITATIONS
91	Duskside auroral undulations observed by IMAGE and their possible association with large-scale structures on the inner edge of the electron plasma sheet. Geophysical Research Letters, 2005, 32, .	4.0	14
92	Realistic magnetospheric density model for 29 August 2000. Journal of Atmospheric and Solar-Terrestrial Physics, 2006, 68, 615-628.	1.6	14
93	Global observations of ring current dynamics during corotating interaction region–driven geomagnetic storms in 2008. Journal of Geophysical Research, 2010, 115, .	3.3	14
94	Localâ€ŧimeâ€dependent lowâ€altitude ion spectra deduced from TWINS ENA images. Journal of Geophysical Research: Space Physics, 2013, 118, 2928-2950.	2.4	14
95	An empirical model for the location and occurrence rate of nearâ€Earth magnetotail reconnection. Journal of Geophysical Research: Space Physics, 2013, 118, 6389-6396.	2.4	14
96	Temperature of the plasmasphere from Van Allen Probes HOPE. Journal of Geophysical Research: Space Physics, 2017, 122, 310-323.	2.4	14
97	The Big Picture: Imaging of the Global Geospace Environment by the TWINS Mission. Reviews of Geophysics, 2018, 56, 251-277.	23.0	13
98	Imaging the Global Distribution of Plasmaspheric Oxygen. Journal of Geophysical Research: Space Physics, 2018, 123, 2078-2103.	2.4	13
99	Recent Progress in Physics-Based Models ofÂtheÂPlasmasphere. , 2009, , 193-229.		13
100	Multiple plasmapause undulations observed by the IMAGE satellite on 20 March 2001. Journal of Atmospheric and Solar-Terrestrial Physics, 2007, 69, 322-333.	1.6	12
101	Possible evidence of virtual resonance in the dayside magnetosphere. Journal of Geophysical Research, 2009, 114, .	3.3	12
102	Latitudinal anisotropy in ring current energetic neutral atoms. Geophysical Research Letters, 2012, 39,	4.0	12
103	First joint in situ and global observations of the mediumâ€energy oxygen and hydrogen in the inner magnetosphere. Journal of Geophysical Research: Space Physics, 2015, 120, 7615-7628.	2.4	12
104	Plasmaspheric drainage plume observed by the Polar satellite in the prenoon sector and the IMAGE satellite during the magnetic storm of 11 April 2001. Journal of Geophysical Research, 2007, 112, n/a-n/a.	3.3	11
105	Determining Plasmaspheric Density From the Upper Hybrid Resonance and From the Spacecraft Potential: How Do They Compare?. Journal of Geophysical Research: Space Physics, 2020, 125, no.	2.4	10
106	Analytical estimate for lowâ€altitude ENA emissivity. Journal of Geophysical Research: Space Physics, 2016, 121, 1167-1191.	2.4	9
107	Composition of 1–128ÂkeV Magnetospheric ENAs. Journal of Geophysical Research: Space Physics, 2018, 123, 2668-2678.	2.4	8
108	Simulations of Van Allen Probes Plasmaspheric Electron Density Observations. Journal of Geophysical Research: Space Physics, 2018, 123, 9453-9475.	2.4	8

#	Article	IF	CITATIONS
109	Magnetosphere dynamics during the 14ÂNovember 2012 storm inferred from TWINS, AMPERE, Van Allen Probes, and BATS-R-US–CRCM. Annales Geophysicae, 2018, 36, 107-124.	1.6	8
110	Pi2 pulsations in a small and strongly asymmetric plasmasphere. Journal of Geophysical Research, 2005, 110, .	3.3	7
111	Multi-spacecraft observations of small-scale fluctuations in density and fields in plasmaspheric plumes. Annales Geophysicae, 2012, 30, 623-637.	1.6	7
112	An improved wide-field camera for imaging Earth's plasmasphere at 30.4 nm. Proceedings of SPIE, 2013, ,	0.8	7
113	On the relation between electric fields in the inner magnetosphere, ring current, auroral conductance, and plasmapause motion. Geophysical Monograph Series, 2005, , 159-166.	0.1	6
114	Direct effects of the IMF on the inner magnetosphere. Geophysical Monograph Series, 2005, , 127-139.	0.1	6
115	Electric Fields and Magnetic Fields in the Plasmasphere: AÂPerspective FromÂCLUSTER andÂIMAGE. Space Science Reviews, 2009, 145, 107-135.	8.1	6
116	Analytical model of rotating twoâ€cell convection at Saturn. Journal of Geophysical Research: Space Physics, 2014, 119, 1980-1993.	2.4	6
117	Multiâ€Instrument Characterization of Magnetospheric Cold Plasma Dynamics in the June 22, 2015 Geomagnetic Storm. Journal of Geophysical Research: Space Physics, 2021, 126, e2021JA029292.	2.4	6
118	Plasmasphere Response: Tutorial and Review of Recent Imaging Results. Space Sciences Series of ISSI, 2006, , 203-216.	0.0	6
119	Multiâ€Scale Density Structures in the Plasmaspheric Plume During a Geomagnetic Storm. Journal of Geophysical Research: Space Physics, 2022, 127, .	2.4	6
120	Terrestrial Energetic Neutral Atom Emissions and the Groundâ€Based Geomagnetic Indices: Implications From IBEX Observations. Journal of Geophysical Research: Space Physics, 2019, 124, 8761-8777.	2.4	5
121	Magnetospheric Convection near a Drainage Plume. Journal of Geophysical Research, 2007, 112, n/a-n/a.	3.3	4
122	The source of the steep plasma density gradient in middle latitudes during the 11–12 April 2001 storm. Journal of Geophysical Research, 2012, 117, .	3.3	4
123	Lowâ€Altitude Emission of Energetic Neutral Atoms: Multiple Interactions and Energy Loss. Journal of Geophysical Research: Space Physics, 2017, 122, 10,203-10,234.	2.4	4
124	Dynamics of a geomagnetic storm on 7–10 September 2015 as observed by TWINS and simulated by CIMI. Annales Geophysicae, 2018, 36, 1439-1456.	1.6	4
125	The Scalable Plasma Ion Composition and Electron Density (SPICED) Model for Earth's Inner Magnetosphere. Journal of Geophysical Research: Space Physics, 2021, 126, e2021JA029565.	2.4	4
126	Plasma Imaging, LOcal Measurement, and Tomographic Experiment (PILOT): A Mission Concept for Transformational Multi-Scale Observations of Mass and Energy Flow Dynamics in Earth's Magnetosphere. Frontiers in Astronomy and Space Sciences, 0, 9, .	2.8	4

#	Article	IF	CITATIONS
127	On the Relation Between Sub-Auroral Electric Fields, the Ring Current and the Plasmasphere. Geophysical Monograph Series, 0, , 163-172.	0.1	3
128	Evidence of <i>m</i> Â=Â1 density mode (plasma cam) in Saturn's rotating magnetosphere. Journal of Geophysical Research: Space Physics, 2016, 121, 2335-2348.	2.4	3
129	Empirical determination of extreme ultraviolet imager background. Journal of Geophysical Research: Space Physics, 2017, 122, 7414-7432.	2.4	3
130	Velocity Rotation Events in the Outer Magnetosphere Near the Magnetopause. Journal of Geophysical Research: Space Physics, 2019, 124, 4137-4156.	2.4	3
131	The Role of the Dynamic Plasmapause in Outer Radiation Belt Electron Flux Enhancement. Geophysical Research Letters, 2020, 47, e2020GL086991.	4.0	3
132	Highâ€Density Magnetospheric He ⁺ at the Dayside Magnetopause and Its Effect on Magnetic Reconnection. Journal of Geophysical Research: Space Physics, 2021, 126, .	2.4	3
133	Electric Fields and Magnetic Fields in the Plasmasphere: AÂPerspective fromÂCLUSTER andÂIMAGE. , 2009, , 107-135.		3
134	Empirical Model of Precipitating Ion Oval. Journal of Geophysical Research: Space Physics, 2017, 122, 10,458-10,471.	2.4	2
135	Nightside Pi2 Wave Properties During an Extended Period With Stable Plasmapause Location and Variable Geomagnetic Activity. Journal of Geophysical Research: Space Physics, 2017, 122, 12,120.	2.4	2
136	Clobal ENA Imaging and In Situ Observations of Substorm Dipolarization on 10 August 2016. Journal of Geophysical Research: Space Physics, 2020, 125, e2019JA027733.	2.4	2
137	Average Ring Current Response to Solar Wind Drivers: Statistical Analysis of 61ÂDays of ENA Images. Journal of Geophysical Research: Space Physics, 2022, 127, .	2.4	2
138	H ⁺ Pitch Angle Distributions in the Outer Magnetosphere Observed by MMS HPCA. Journal of Geophysical Research: Space Physics, 2022, 127, .	2.4	2
139	Progress in understanding the inner magnetosphere. Eos, 2012, 93, 348-348.	0.1	1
140	Empirical Characterization of Lowâ€Altitude Ion Flux Derived from TWINS. Journal of Geophysical Research: Space Physics, 2018, 123, 3672-3691.	2.4	1
141	Localizing Sources of Pc1 Geomagnetic Pulsations. Bulletin of the Russian Academy of Sciences: Physics, 2021, 85, 334-339.	0.6	1
142	Relative Timing of Nightside and Dayside Plasmapause Motion: Two Events in June 2001. Journal of Geophysical Research: Space Physics, 2020, 125, e2019JA027153.	2.4	0
143	The future of plasmaspheric extreme ultraviolet (EUV) imaging. , 2022, , 231-286.		0